JAERI-M
83-200

ELECTRON PROBE MICRO-ANALYSIS OF IRRADIATED TRISO-COATED UO_2 PARTICLES (I)

November 1983

Toru OGAWA, Kazuo MINATO, Kosaku FUKUDA
and Katsuichi IKAWA

日本原子力研究所
Japan Atomic Energy Research Institute

JAERI-Mレポートは，日本原子力研究所が不定期に公刊している研究報告書です。
入手の問合わせは，日本原子力研究所技術情報部情報資料課（〒319-11茨城県那珂郡東海村）あて，お申しこしください。なお，このほかに財団法人原子力弘済会資料センター（〒319-11 茨城県那珂郡東海村日本原子力研究所内）で複写による実費頒布をおこなっております。

JAERI-M reports are issued irregularly.
Inquiries about availability of the reports should be addressed to Information Section, Division of Technical Information, Japan Atomic Energy Research Institute, Tokai-mura, Naka-gun, Ibaraki-ken 319-11, Japan.

©Japan Atomic Energy Research Institute, 1983

編集兼発行　日本原子力研究所
印　　刷　㈱高野高速印刷

JAERI-M 83-200

Electron Probe Micro-Analysis of Irradiated Triso-Coated UO_2 Particles (I)

Toru OGAWA, Kazuo MINATO, Kosaku FUKUDA
and Katsuichi IKAWA

Department of Fuels and Materials Research, Tokai Research Establishment, JAERI

(Received October 29, 1983)

The Triso-coated low-enriched UO_2 particles were subjected to the post-irradiation electron probe micro-analysis. Observations and analyses on the amoeba effect, inclusions and solutes in the UO_2 matrix were made. In the cooler side of the particle which suffered extensive kernel migration, two significant features were observed: (1) the wake of minute particles, presumably UO_2, left by the moving kernel in the carbon phase and (2) carbon precipitation in the pores and along the grain boundaries of the UO_2 kernel. Both features could be hardly explained by the gas-phase mechanism of carbon transport and rather suggest the solid state mechanism. Two-types of 4d-transition metal inclusions were observed: the one which was predominantly Mo with a fraction of Tc and another which was enriched with Ru and containing significant amount of Si. The Mo and Si were also found in the UO_2 matrix; the observation led to the discussion of the oxygen potential in the irradiated Triso-coated UO_2 particle.

Keywords: Triso-Coated Particle Fuel, UO_2, Fission Products, Kernel Migration, Electron Probe Micro-Analysis, Post-irradiation Examination, Amoeba Effect, Inclusion

JAERI－M 83－200

照射済Triso 被覆UO_2 粒子のEPMA－(I)

日本原子力研究所東海研究所燃料工学部
小川　徹・湊　和生・福田　幸朔・井川　勝市

（１９８３年１０月２９日受理）

Triso 被覆低濃縮UO_2 粒子の照射後EPMAを行い，アメーバ効果，UO_2 中のFP 析出物・溶質について観察・分析した。著しい核移動を示した粒子の低温側の観察からは，次に示す２つの特徴を見出した。1)炭素析出相中に，UO_2 核の移動の跡を示す微細粒子が分布していた。これら微細粒子はUO_2 と考えられる。2)UO_2 核中の気孔および粒界に炭素が析出していた。これらの特徴は炭素の気相輸送モデルによっては説明困難であり，むしろ固相輸送機構を示唆するものである。４d 遷移金属合金相としては２種類が見出された。１つは小量のTc を含むMo 相であり，他はRu とSi とを多く含む相である。Mo とSi はUO_2 母相中にも見出された。後者の観察から，Triso 被覆Uo_2 粒子中の照射下の酸素ポテンシャルを議論した。

CONTENTS

1. Introduction 1
2. Experimental 2
2.1 Instrumentation 2
2.2 Standards 3
2.3 Samples 3
3. Results and discussion 5
3.1 Unirradiated particles 5
3.2 Irradiated particles 7
3.2.1 Amoeba effect 7
3.2.2 Fission-product precipitates 9
3.2.3 Fission products in UO_2 matrix 12
4. Conclusion 14
Acknowledgements 15
References 16

目　　次

1. 序　論 …… 1
2. 実　験 …… 2
2.1 装　置 …… 2
2.2 標準試料 …… 3
2.3 試　料 …… 3
3. 結果と考察 …… 5
3.1 未照射粒子 …… 5
3.2 照射粒子 …… 7
3.2.1 アメーバ効果 …… 7
3.2.2 核分裂生成物析出物 …… 9
3.2.3 UO_2 母相中の核分裂生成物 …… 12
4. 結　論 …… 14
謝　辞 …… 15
参考文献 …… 16

LIST OF TABLES

Table 1 Irradiation data of coated fuel particles employed for electron probe micro-analysis.

Table 2 List of standard samples.

Table 3 Examples of EPMA studies on chemical states of fission products in the oxide fuel.

Table 4 Results of quantitative analysis of Mo. Oxygen potential was calculated by assuming Mo detected in the UO_2 matrix as solute.

LIST OF FIGURES

Fig. 1 Relative intensity of $L_{\alpha 1}$ X-ray as a function of atomic number.

Fig. 2 Irradiation history of 74FC1-3A particles.

Fig. 3 Schematic representation of Triso-coated fuel particle employed in the study.

Fig. 4 Epoxy-resin mould for sample preparation.

Fig. 5 X-ray spectrum from the alloy inclusion of unirradiated 74UC1 particle.

Fig. 6 X-ray spectrum from the UO_2 matrix of unirradiated 74FC1 particle.

Fig. 7 Energy dispersive X-ray spectrum from the metallic inclusion of unirradiated 74FC1 particle heated at 2100°C for 1 hr.

Fig. 8 Observation on the cooler side of the amoeba particle (74FC1-3A).

Fig. 9 Schematic representation of the carbon phase accumulated in the cooler side of the particle.

Fig. 10 Photomicrographs of 74FC1-3A particles (ref.(4)).

Fig. 11 Back-scattered electron topograph of the carbon phase.

Fig. 12 Carbon precipitates in the pores of UO_2 matrix of 74FC1-3A particle.

Fig. 13 Carbon precipitates along the grain boundaries of UO_2 kernel of 74UC1-3B particle.

Fig. 14 X-ray spectra from the alloy inclusions of 74FC1-3A particle.

Fig. 15 X-ray spectra at the point of Si peak of the inclusion of Fig. 14b. a)EDX, b)WDX.

Fig. 16 Phase diagram of Mo-Ru(Tc)-$Rh_{0.5}Pd_{0.5}$ pseudo-ternary system[16]. Asterisk shows the approximate position expected for 74FC1-3A particle. Partial oxidation of Mo would shift the composition as shown by arrow.

Fig. 17 Si distribution in 74FC1-3A particle.

Fig. 18 Account of oxygen balance in the particles 74FC1-3A and 5A.

1. Introduction

For full understanding of the irradiation performance of coated particle fuel, it is pertinent to know the chemical reactions taking place within it. Pressure vessel failure and kernel migration, for instance, of coated UO_2 particles are related to the $CO+CO_2$ pressure build-up or the oxygen potential within the particles. Knowledge on the chemical states of various fission products would facilitate understanding the process of fission-product release in both normal and accident conditions. Besides, the SiC corrosion by fission-product Pd would be determined not only by the thermochemistry of the system Pd-SiC but also by the behavior of Pd within UO_2.

Electron probe micro-analysis (EPMA) of irradiated coated fuel particles is expected to give the relevant knowledge. The shielded electron probe microanalyzer in JMTR hot laboratory has been used to analyze the irradiated Triso-coated UO_2 particles. In this paper the observations restricted within the UO_2 kernel is reported; those on the fission products within the coating shall follow as a separate paper.[1] The analyses performed to date are nothing but preliminary. The more detailed study is due in the series of EPMA examinations on schedule.

2 Experimental

2.1 Instrumentation

The shielded electron probe microanalyzer is the type JEOL-JRXA 501 which has been designed on the basis of JEOL 501 to handle specimens containing up to 10 Ci of 0.8 MeV gamma radiation with the dose at the instrument surface below 1 mR/h. Appropriate shielding is also provided for the X-ray spectrometers, secondary-electron detector etc. The instrument is equipped with both wavelength-dispersive and energy-dispersive spectrometers. The wavelength-dispersive system (WDX) is composed of two-channels, each containing three diffracting crystals, thus capable of analyzing elements from B to Am. The energy dispersive spectrometer (EDX) consists of a Si(Li) detector connected to a microcomputer, which can rapidly identify the elements from Na to Am. Quantitative analysis could be performed by the microcomputer on the information from both on-line EDX and off-line WDX. The EDX has a disadvantage of comparatively poor resolution in analyzing multi-component materials such as fission-product precipitates in which several elements neighboring in the periodical table appear. Hence the EDX was used for rapidly locating analyzing points and economizing the machine time; the detailed examination was done by the WDX.

For visual observation we could rely on the secondary, back-scattered (composition and topography), and absorbed electron images as well as the X-ray images. The principles of X-ray spectrometries and the meaning of these images are described in refs. (2, 3).

2.2 Standards

Sample holder could accomodate maximum ten standard samples along with the sample to be analyzed. Standard samples listed in Table 2 were prepared. Since metals and oxides of the alkaline earth and rare earth elements, except CeO_2, are hygroscopic, the standards containing these elements were prepared as zirconates. The $CsAl(SO_4)\cdot 12H_2O$ is the less hygroscopic among chemically unstable compounds of Cs. Suitable sample of pure Ru was not obtainable; Ru powder was melted with excess Si to form Ru_2Si_3+Si. The X-ray intensity for pure Ru was calculated from that obtained on Ru_2Si_3 grain. Intensities for pure Tc and Rh were interpolated as shown in Fig. 1.

2.3 Samples

Samples were the Triso-coated UO_2 particles irradiated in JMTR capsule 73F13A. The capsule was irradiated in the fuel zone for six JMTR cycles (111 effective full power days). The maximum fast fluence and burnup amounted to 2.7×10^{21} n/cm^2 (>0.18 MeV) and 5.3% FIMA, respectively. Fig. 2 depicts the irradiation history of the 74FC1-3A particles. Irradiation temperature was lowered after 50 efpd because of the malfaction of the thermocouple for temperature control. Table 1 summarizes irradiation temperature, burnup, fast fluence etc for the sample particles. Standard size of the particles is illustrated in Fig. 3. The detail of irradiation and post irradiation examination of 73F13A capsule is treated in elsewhere.[4)]

Five or ten particles each were embedded in epoxy resin employing a mould shown in Fig. 4. The samples were then polished to the equator by a usual hot-laboratory ceramographic techniques. Washing was made with water, which, however, might have a deleterious effect on some chemically active species such as Cs compounds. Other appropriate solvent should be sought for the analyses in future. Gold was vapor deposited on the polished surface to prevent the sample from charging during the analysis.

3. Results and discussion.

3.1 Unirradiated particles

Unirradiated particles 74FC1 and 74UC1 were analyzed to certify the initial condition. The kernel of 74FC1 was fabricated by Nuclear Fuel Industry with a sol-gel techniques and that of 74UC1 by UKAEA Springfields Works with powder agglomeration techniques. According to the commercial certificates, the kernel of 74FC1 contained 100 ppm Si as the most abundant impurity, while that of 74UC1 had 120 ppm Fe and 17 ppm Cr, which would have been picked up during powder agglomeration.

The energy dispersive analysis on 74UC1 revealed a small amount of Fe-Cr-Si alloy particles included in the UO_2 matrix (Fig. 5). On the other hand, no inclusions were observed within the kernel of 74FC1. Fig. 6 shows the X-ray spectrum from UO_2 matrix of the latter, in which only U peaks are evident.

Unirradiated 74FC1 particles heated at 2100°C for 1h was also analyzed. Small white inclusions at the grain boundaries of UO_2 has been observed on the Triso-coated particles heated to such high temperatures.[5,6] Though the inclusions have been considered to be metal U precipitated on cooling from the UO_2 matrix, which dissociated oxygen and became hypostoichiometric at very high temperatures, the analysis showed the inclusion to be containing an appreciable amount of Si (Fig. 7). However, the inclusions were too minute to be submitted to quantitative analysis: it was almost impossible to remove the uranium X-ray from the matrix itself. The observation suggests that the reaction between UO_{2-x} and Si be taken into account in discussing

the behavior of Triso-coated UO_2 particles at very high temperatures. The Si would have been supplied by the dissociation of the SiC coating in addition to the impurity initially present in UO_2.

3.2 Irradiated particles

3.2.1 Amoeba effect

The 74FC1-3A and 74UC1-3B particles had experienced irradiation at about 1650°C for 30 days out of 111 efpd. Extensive kernel migration or amoeba effect occurred to bring about high failure fractions seen in Table 1. Fig. 8 shows the secondary and back-scattered electron images as well as the X-ray images of U, C and O of the cooler side of the amoeba particle (74FC1-3A). One can see the wake of minute particles left by the moving UO_2 kernel in the sea of carbon. Also one can infer from the uranium and oxygen images that these minute particles are UO_2 rather than UC_2 or UC. The carbon phase accumulated in the cooler side could be considered to consist of three regions separated by two disconnecting planes; the separation is distinguished by the distribution of the minute particles, as schematically shown in Fig. 9. The irradiation history given in Fig. 2 suggests that each of the three regions corresponds to each of the three periods at about 1650°C. Such an observation would be useful in tracing the kernel migration history during a fuel life.

The distribution of the minute particles was hardly discernible under the optical microscopy (Fig. 10).[4] Since the region densely populated by the minute particles was harder than the surrounding carbon, the carbon phase developed an apparent structure by polishing, as seen in the back-scattered electron topograph in Fig. 11. Besides, owing to the minute particles, the carbon phase became seemingly active to the polarized light as if in a stage of graphitization (Fig. 10C). Thus one should

be cautious in inferring a carbon transport mechanism from optical microstructural evidences.

Figs. 12 and 13 indicate carbon precipitates within the pores and along the grain boundaries of UO_2, suggesting that the carbon is transported by the solid state diffusion in UO_2 matrix. Similar observations have led to the postulation of a solid state mechanism in the coated ThO_2 particles[9]. The gas phase transport mechanism would hardly explain both the presence of the minute particles, of UO_2 presumably, in the carbon phase and the carbon inclusion within the UO_2 kernel.

3.2.2 Fission-product precipitates

There have appeared several EPMA studies on the chemical states of fission products in the oxide fuel[8-16]. However, there are so many factors, such as initial composition, burnup, fission spectrum and temperature, playing roles in determining the chemical behavior of fission products that many aspects of the problem are not resolved yet. And precaution is necessary in applying the knowledge obtained on a sample having different character and irradiation history. Several EPMA studies on the oxide fuel appeared in the literature are summarized in Table 3. The studies on coated fuel particles have employed high-enriched high-burnup samples. Most of the others examined MO_x fuel for FBR, except those by Bradbury et al.[9,10] on medium and low-enriched UO_2. Bradbury et al. have distinguished two types of fission-product precipitates: the Ba-containing and the Ba-free. Today, it is widely accepted that the Ba-containing phase is the perovskite-type mixed oxide and the Ba-free phase is the alloy of 4d-transition metals from Mo to Pd. Besides, Pd-Ag-Cd[15], Pd-Te-Sn[11,12], U-Pu-Ru-Rh-Pd[11] alloys or compounds have been identified in restricted conditions.

In the present study, however, the Ba-containing phase was not found. Bradbury et al. have found only eighty Ba-containing precipitates out of 3700 precipitates examined. Therefore, even if the solubility of BaO in UO_2 is negligibly small[17], it would not be strange that we could not find a Ba-containig precipitate, because number of precipitates of visible size (~1μm) was only about fifty and that suitable for analysis was even smaller in

a particle. And it is hard to distinguish the oxide inclusion in the oxide matrix under the optical microscopy. It is also hard to find the minute precipitate of lighter elements in the matrix of the heavier elements in the electron images.

On the other hand, we found the two kinds of alloy precipitates in the particle 74FC1-3A. Wavelength dispersive X-ray spectrum in Fig. 14a was taken on an alloy precipitate. The precipitate was composed of predominantly Mo with a small amount of Tc. Another type of precipitates, whose X-ray spectrum is in Fig. 14b, consisted of Mo, Tc, Ru, Rh and Pd; Si was also detected when using TAP diffracting crystal. The latter proved to be a composite of at least two different phases: two different X-ray spectra were obtained on slightly different positions of the same precipitate (Fig. 15). The two phases were considered to be Mo-base alloy like that in Fig. 14a and, presumably, Ru-base silicide.

From the burnup and the percent fissions in Pu of the sample, the composition in the system Mo-Tc-Ru-Rh-Pd would be approximately that marked by asterisk in Fig. 16. An amount of Mo, however, had been oxidized (see 3.2.3) to shift the composition as shown by the arrow in the figure. Thus, in the absence of Si, the alloy may be in the phase field of either $\sigma + \varepsilon$ or ε. Considering the constitutions of binary systems Mo-Ru[18], Mo-Si[19], Ru-Si[20] and the heats of formation of σ phase[21] and relevant silicides[22], one predicts that the addition of Si to the ε phase of the Mo-Ru system would result in the formation of Ru_2Si. Therefore, the addition of Si to the five component $\sigma + \varepsilon$ or ε would also produce a silicide in which Ru is one of the major constituents. Thus, a part of the

observation is explained, but the problem remains: the composition of the alloy phase of Fig. 14a corresponds to that of β phase rather than σ or ε, the latters of which are expected to be the residue of the reaction between Si and the $\sigma + \varepsilon$ or ε. Obviously the knowledge on the multicomponent equilibria consisting of Si and the transition metals is not enough to make the detailed discussion about the present observation.

The Si would have been generated by either the dissociation of SiC or the reaction of CO with SiC to form volatile SiO. The migration of Si from the SiC coating into the kernel is evident in Fig. 17; also the Si peaks at the alloy precipitates indicated by the Mo peaks.

For 74FC1-5A particles irradiated at temperatures lower than those of 74FC1-3A particles, only the usual 4d-transition metal alloy phase containing Mo, Tc, Ru, Rh and Pd but not Si was found.

3.2.3 Fission products in UO_2 matrix

The quantitative analyses were made for Nd, Zr, Mo and Si in the UO_2 matrix. The Nd was investigated for its possibility as a burnup monitor. The Zr was analyzed to see whether the element remained in the matrix or partially segregated as a $BaZrO_3$-type phase. After an appropriate correction for the spectra obtained on the 74FC1-5A particle, ratios Nd/U and Zr/U were found to be 0.006 and 0.009, respectively. Both values were lower by about 20% than those expected for the sample. The differences might be ascribed to the experimental errors, because there remain the problems in the selection of proper measuring condition and the preparation of the standard sample, sintered $Nd_2Zr_2O_7$. However, if Zr ever segregates as $BaZrO_3$, it will be only about 20% of the total Zr, since the fission yield of Ba is about the fraction of that of Zr. Therefore, the present range of experimental error is too large to deduce the meaningful conclusion about the distribution of Zr.

The solubility of MoO_2 in UO_2 seems controversial. Johnson et al. have recognized up to 0.3 mol% of MoO_2 in the irradiated $(U,Pu)O_2$ matrix[24], but out-of-pile simulation experiments[14,23] have shown a very limited solubility ($\lesssim$0.02 at% Mo). And Kleykamp has ascribed the Mo detected in the oxide fuel matrix to the finely dispersed almost invisible particles or microsegregations of the perovskite-type oxides[16]. Though the ambiguity exists in this respect, Table 4 gives the results of quantitative analyses, regarding Mo as dissolving in UO_2 rather than component of microsegregations. The point analysis

was made at about the center of the kernel.

Johnson et al. have employed Mo as in-situ redox indicator to deduce the oxygen potential of the system[15,24]:

$$\Delta\bar{G}_{O_2} = RT\ln P_{O_2} = G^{\circ}_{f\ MoO_2} + RT\ln x_{MoO_2} - RT\ln x_{Mo} + RT\ln \gamma_{MoO_2}/\gamma_{Mo}$$

where x_{MoO_2} and x_{Mo} are the mole fractions of MoO_2 in UO_2 and that of Mo in the alloy phase, respectively; the γ's are the relevant activity coefficients. The oxygen potential in Table 4 was calculated by assuming $\gamma_{MoO_2}/\gamma_{Mo}$ to be unity. The error in $\gamma_{MoO_2}/\gamma_{Mo}$ by factor five causes that in $\Delta\bar{G}_{O_2}$ of about 4 kcal/mol. The corresponding CO pressures were calculated by assuming the carbon activity to be unity because of the carbon coating.

Simple theoretical consideration of the oxygen balance in the irradiated UO_2, in which oxidation of alkaline earths, Zr, Y and rare earths is taken into account, gives CO pressures much higher than those in Table 4 [25,26]. In Fig. 18, the oxygen balance was recalculated considering the oxidation of Mo and Si as well as the above elements; there will be hardly any excess of oxygen to produce CO if Y and rare earths should exist as tetravalent oxides. And it is interesting to note that the amount of oxydized Mo and Si was smaller for the sample experienced higher temperatures (74FC1-3A). The fact would be related to the formation of the Si-containing transition metal phase in this particle, as seen in 3.2.2.

Table 4 also shows the CO pressures predicted by the experimental equation for the oxygen release from the irradiated UO_2 by Proksch et al.[27], which agree well with those estimated by the redox method above.

4. Conclusion

The Triso-coated UO_2 particles were subjected to the post-irradiation EPMA examination. This was the first of the series of EPMA study on schedule and the objective was rather to locate the field of the future study.

Observation and analyses on the amoeba effect, inclusions and solutes in the UO_2 matrix were made. In the cooler side of the particle which suffered extensive kernel migration, we observed two significant features: (1) the wake of minute particles, presumably UO_2, left by the moving kernel in the carbon phase and (2) the carbon inclusion in the pores and along the grain boundaries of the UO_2 matrix. Both features would be hardly explained by the gas-phase mechanism of carbon transport and rather suggest the solid state mechanism.

The Ba-containing oxide precipitates was not found in the kernel of the present samples. However, in the particle irradiated at 1650°C at maximum, two types of 4d-transition metal precipitates were observed: the one which was predominantly Mo with a fraction of Tc and another which was enriched with Ru and containing significant amount of Si, presumably a Ru-base silicide. The Mo and Si were also found in the UO_2 matrix. The latter observation led to the discussion of the oxygen potential and CO pressure in the irradiated Triso-coated UO_2 particle.

Acknowledgements

We wish to acknowledge the laborious works by the personnel of Hot Laboratory, Department of JMTR Project, Oarai Research Establishment. Operation of EPMA was done by Mr. M. Shimizu and Mr. Y. Tayama. Thanks are also due to the personnel of Hot Laboratory, Department of Research Reactor Operation, Tokai Research Establishment, for their cooperation in the sample preparation.

We also wish to thank Dr. K. Iwamoto, Director of Department of Fuels and Materials Research, for encouragement.

References

1. K. Minato et al., to be submitted.
2. I. Uchiyama et al., " X-ray Microanalyzer", Nikkan-kogyo-shinbunsha (1972).
3. T. D. Mckinley et al. eds.,"The Electron Micoprobe", Wiley, New York (1966)
4. K. Fukuda et al., to be submitted.
5. A. Naoumidis, Juel-1465(1977).
6. T. Ogawa and K. Ikawa, J. Nucl. Mater. 99(1981)85.
7. C. L. Smith, GA-A14058(1976)
8. J. I. Bramman et al., J. Nucl. Mater. 25(1968)201.
9. B. T. Bradbury et al., AERE-R4845(1965).
10. B. T. Bradbury et al., AERE-R5149(1966).
11. H. Kleykamp, in "Behavior and Chemical State of Irradiated Fuels", IAEA, Vienna (1974), p. 157.
12. R. Foerthmann et al., in "Thermodynamics of Nuclear Materials 1974, vol.I", IAEA, Vienna (1975), p. 147.
13. C. B. Scott et al., Gulf-Ga-B12409(1973).
14. J. O. A. Paschoal, KfK 3473(1983).
15. C. E. Johnson, in "Physical Aspect of Electron Microscopy and Microprobe Analysis", B. M. Siegel and D. R. Beaman Eds., Wiley, New York(1975), p. 373.
16. H. Kleykamp, J. Nucl. Mater. 66(1977)292.
17. E. J. McIver, cited by P. E. Potter in "Behavior and Chemical State of Irradiated Fuels", IAEA, Vienna (1974), p. 115.
18. R. P. Elliot, "Constitution of Binary Alloys, First Supplement", McGraw Hill, New York(1965).
19. T. G. Chart, Metal Science 8(1974)344.

20. W. Obrowski, Metalwissenschaft u. Technik 19(1965)741.
21. L. Brewer and R. H. Lamoreaux, in "Molybdenum: Physico-Chemical Properties of its Compounds and Alloys" (L. Brewer et al., eds.), Atomic Energy Review, special issue No.7, (1980).
22. T. G. Chart, High-Temp.- High Press. 5(1973)241.
23. G. Giacchetti and C. Sari, Nucl. Technol. 31(1976)62.
24. I. Johnson et al., J. Nucl. Mater. 48(1973)21.
25. R. H. Flowers and G. W. Horsley, AERE-R5949(1968)
26. T. Ogawa et al., submitted to JAERI-M.
27. E. Proksch et al., J. Nucl. Mater. 107(1982)280.

Table 1 Irradiation data of coated fuel particles employed for electron probe micro-analysis.

Holder	3A	3B	5A	5B
Sample	74FC1	74UC1	74FC1	74FC1H[b]
Burnup(%FIMA)	4.4	5.3	3.9	3.9
%fission in Pu	26	32	23	22
Fast fluence (cm^{-2}, E > 0.18MeV)	3.1×10^{21}	3.1×10^{21}	2.7×10^{21}	2.7×10^{21}
ϕ_{EOL}[a]	5×10^{-4}-7×10^{-3}	0.1-0.2	$\leq 3\times10^{-3}$	$\leq 5\times10^{-3}$

a) 95% confidence limit of through-coating failure fraction by X-ray microradiography.
b) 74FC1 heated at 1800°C before irradiation.

Table 2 List of standard samples.

Element	Form	Preparation
Sr	$SrZrO_3$	Reaction between $SrCO_3$+ZrO_2.
Ba	$BaZrO_3$	Reaction between $BaCO_3$+ZrO_2.
La	$La_2Zr_2O_7$	Coprecipitation of hydroxides and calcination.
Nd	$Nd_2Zr_2O_7$	
Ce	CeO_2	Commercial.
Cs	$CsAl(SO_4)\cdot 12H_2O$	Precipitation from solution of potassium alum and CsCl.
Ru	Ru_2Si_3+Si	Melting of Ru and Si.
Pd	wire.	
Mo	wire.	

Table 3 Examples of EPMA studies on chemical states of fission products in the oxide fuel.

Author	Sample Composition	%eU	Form	Reactor	Burnup(%FIMA)	Temperatre(°C)
Bramman et al.[8]	$U_{0.85}Pu_{0.15}O_2$		Vipac	DFR	8	$T_{mp}>T_c>2000$
Bradbury et al.[9,10]	UO_2	30	Pellet	Pluto	4.6	1000-1450
		5.5		NRX	0.3	T_c=1970
Kleykamp[11]	$(U,Pu)O_{2-x}$		Pellet	FR2,BR2,DFR	~5	$T_c>T_{mp}$
Foerthmann et al.[12]	UO_2	90	cpf	FRJ2	50	1150-1300
Kleykamp[16]	$(U,Pu)O_{2-x}$		Pellet		≤7	$T_c>T_{mp}$
Paschoal[14]	$(U,Pu)O_{2-x}$		Pellet	FR2,BR2,DFR, Rapsodie	13	T_h=500-700
Scott[13]	UO_2		cpf		>60	870-1460

T_c: temperature at the center

T_h: temperature at the clad inner surface.

T_{mp}: melting point of UO_2

Table 4 Results of quantitative analysis of Mo. Oxygen potential was calculted by assuming Mo detected in the UO_2 matrix as solute.

T(K)[a]	$x_{MoO_2}(UO_2)$	x_{Mo}(alloy)	$\Delta\bar{G}_{O_2}$(kcal/mole)	P_{CO}(atm)[b]	P_{CO}(atm)[c]
1050	0.0094	0.3	-104	0.2	0.9
1230	0.0046	1	-102(±4)	2±2	3.4

a) Irradiation temperature in the latter half of fuel life.

b) $RT\ln P_{CO} = -\Delta G_f^\circ(CO) - \frac{1}{2}\Delta\bar{G}_{O_2}$

c) By the empirical equation for the oxygen release by Proksch et al.[27]

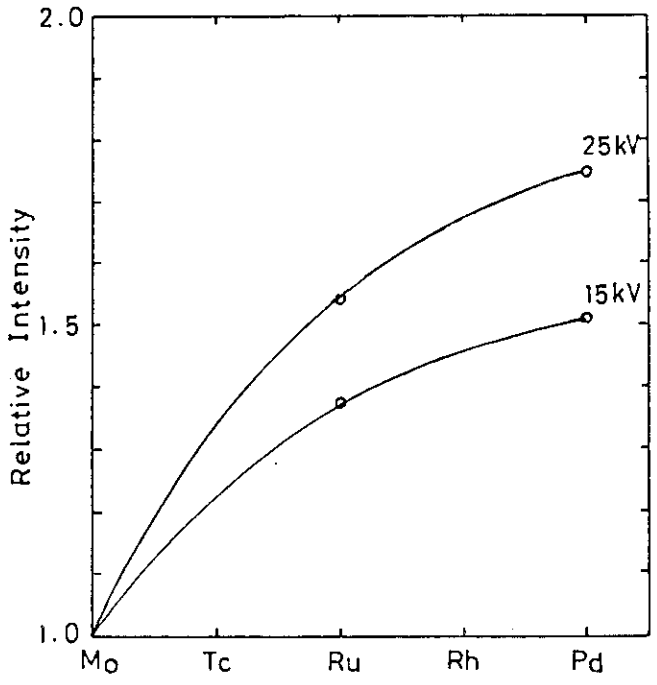

Fig. 1 Relative intensity of $L_{\alpha 1}$ X-ray as a function of atomic number.

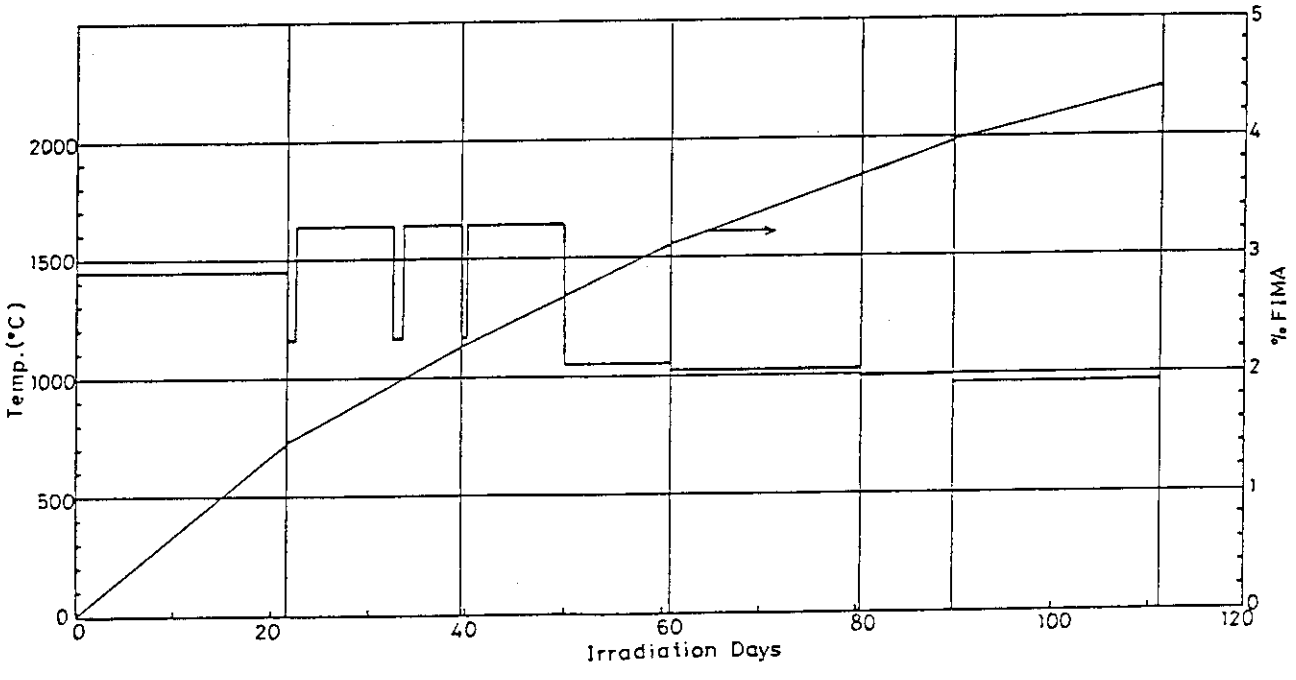

Fig. 2 Irradiation history of 74FC1-3A particles.

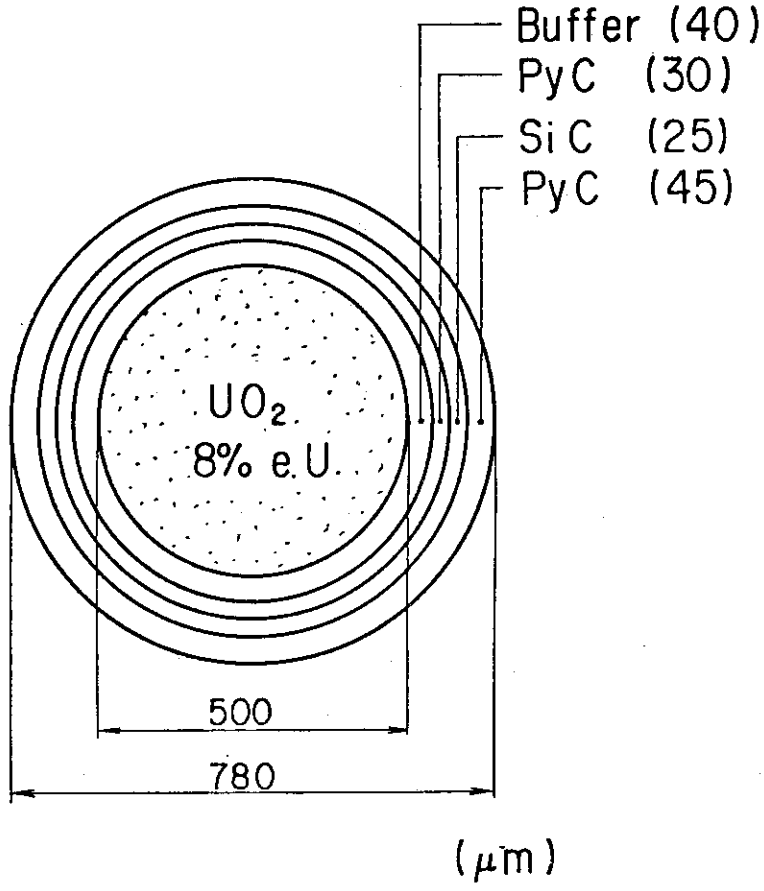

Fig. 3 Schematic representation of Triso-coated fuel particle employed in the study.

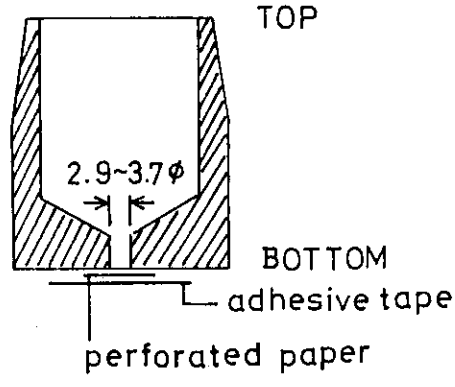

Fig. 4 Epoxy-resin mould for sample preparation.

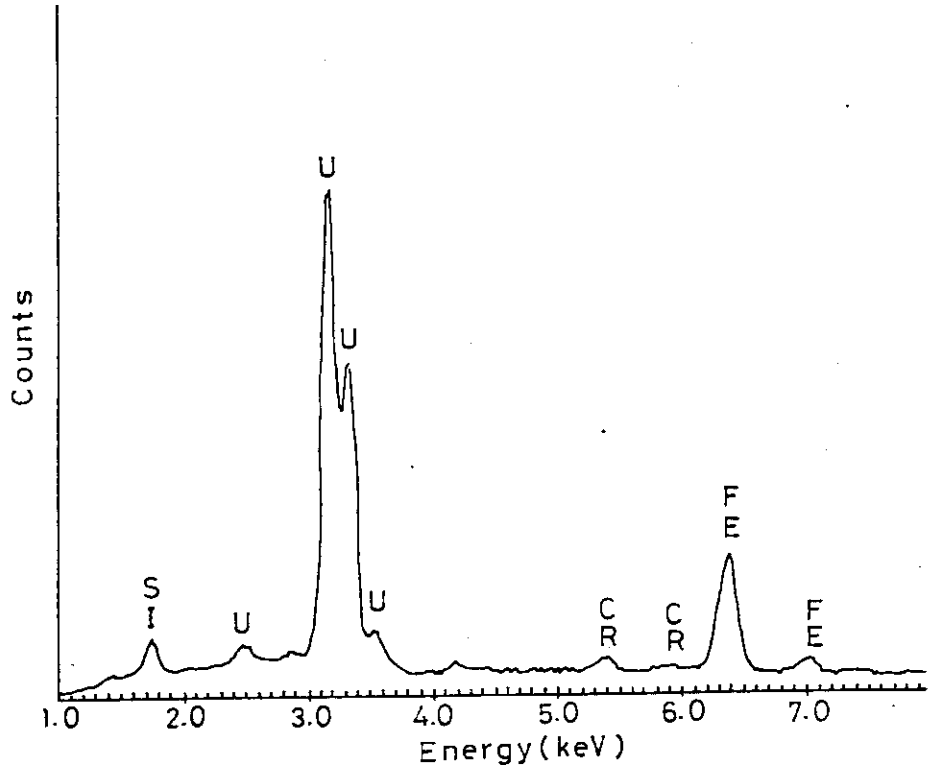

Fig. 5 X-ray spectrum from the alloy inclusion of unirradiated 74UC1 particle.

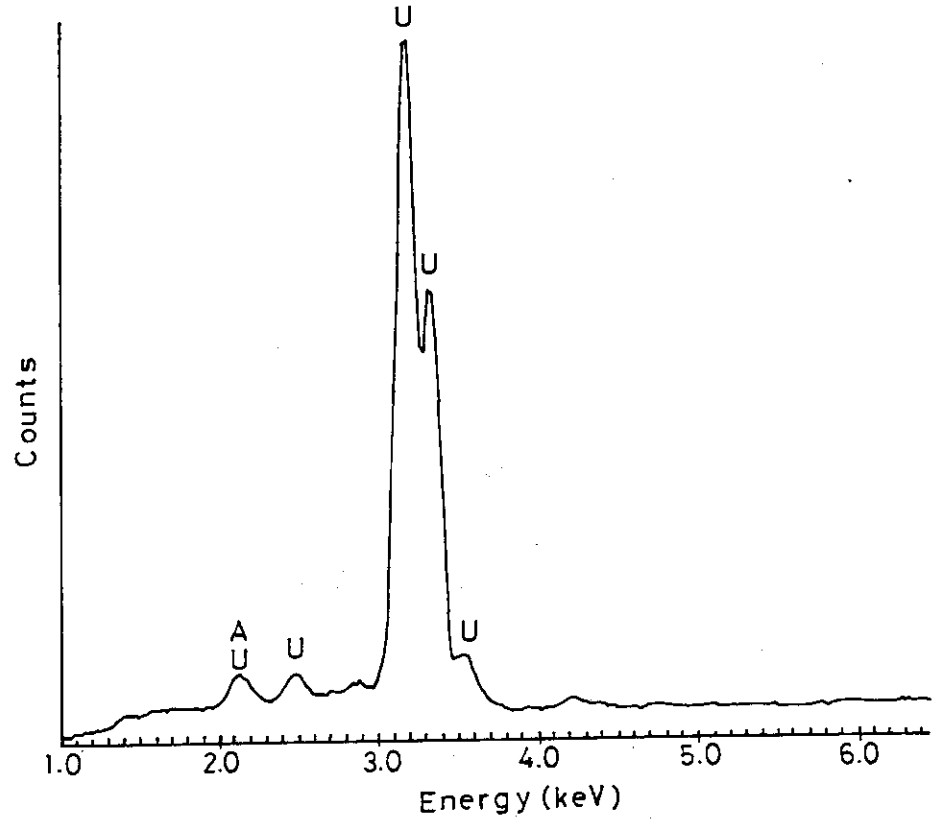

Fig. 6 X-ray spectrum from the UO_2 matrix of unirradiated 74FC1 particle.

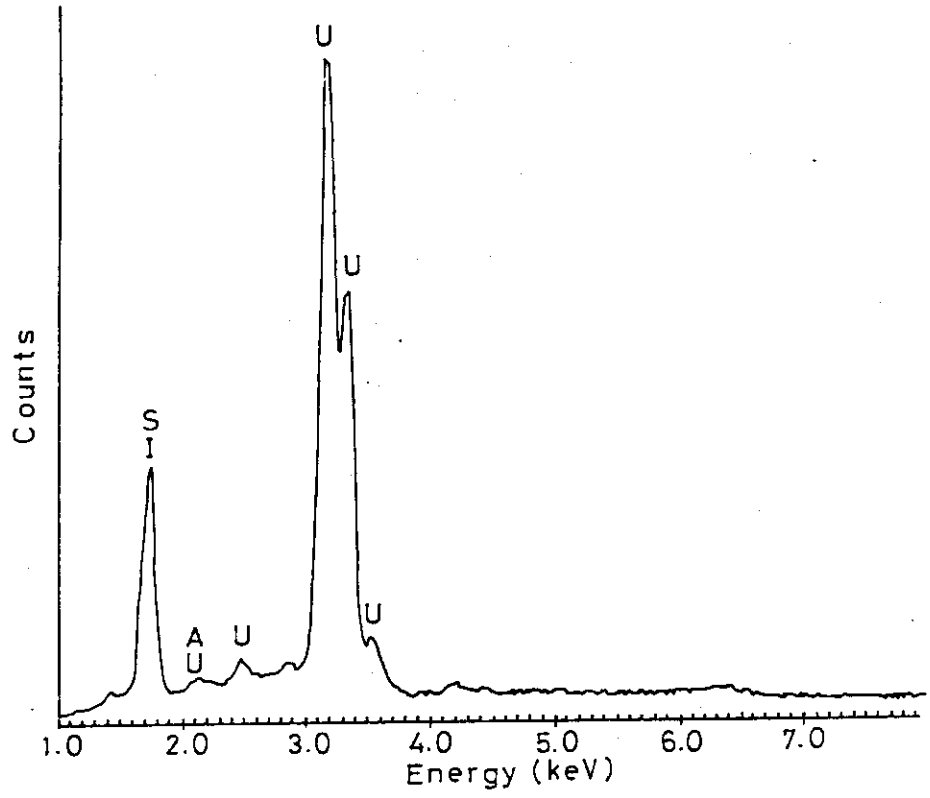

Fig. 7 Energy dispersive X-ray spectrum from the metallic inclusion of unirradiated 74FCl particle heated at 2100°C for 1 hr.

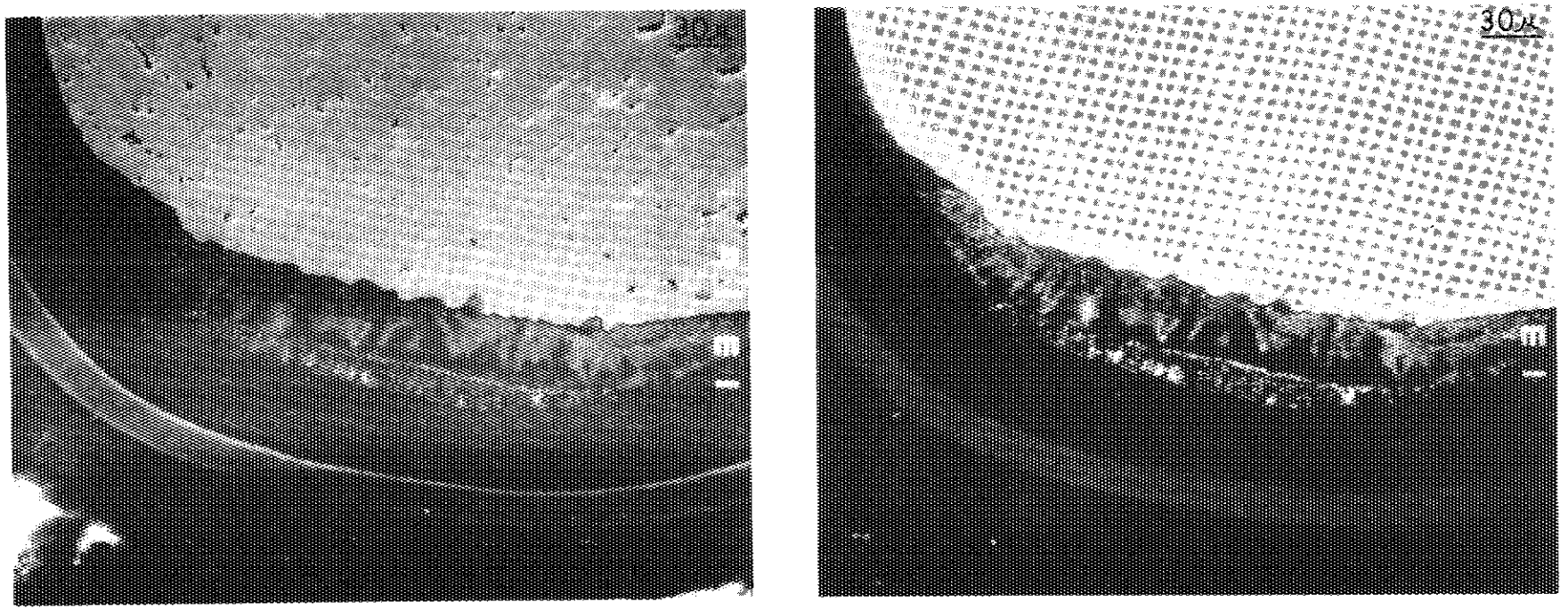

SEI　　BEI

Fig. 8　Observation on the cooler side of the amoeba particle (74FC1-3A).

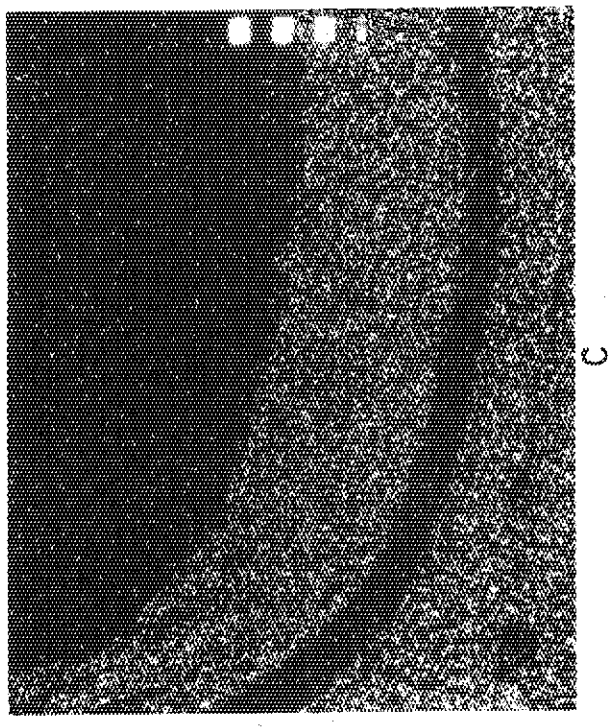

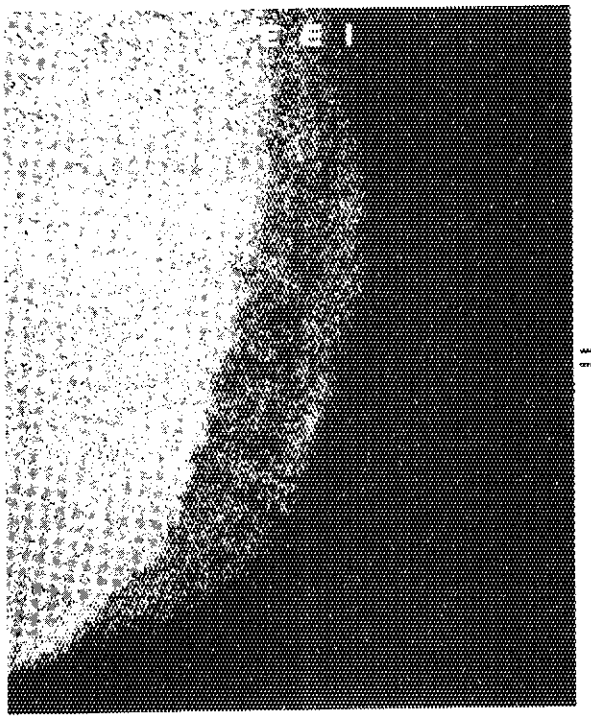

Fig. 8 (continued)

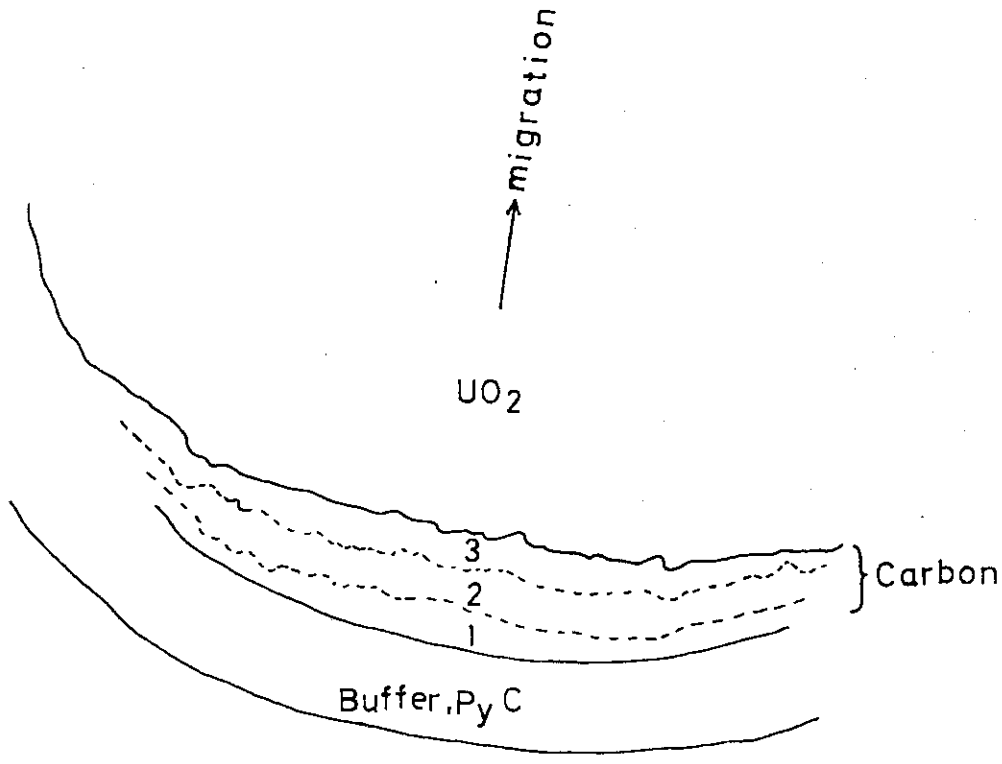

Fig. 9 Schematic representation of the carbon phase accumulated in the cooler side of the particle.

Fig. 10 Photomicrographs of 74FC1-3A particles (ref.(4)).

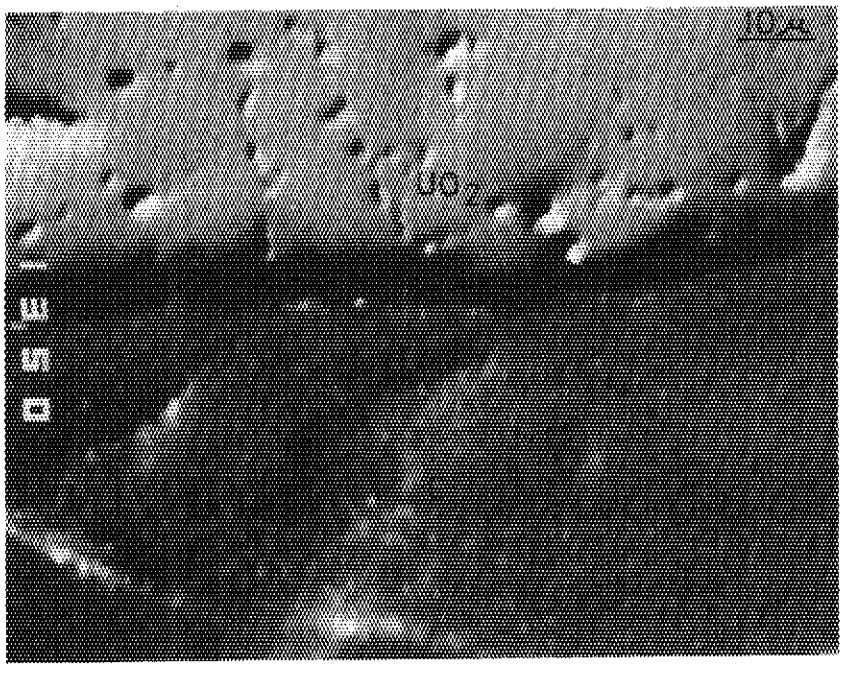

Fig. 11 Back-scattered electron topograph of the carbon phase.

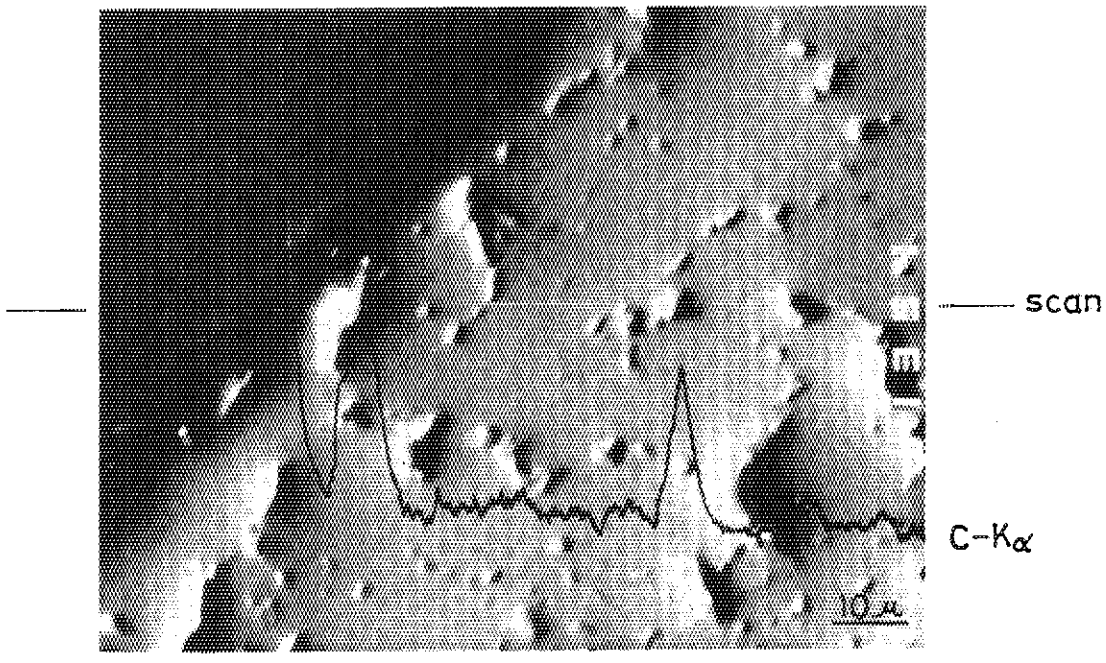

Fig. 12 Carbon precipitates in the pores of UO_2 matrix of 74FC1-3A particle.

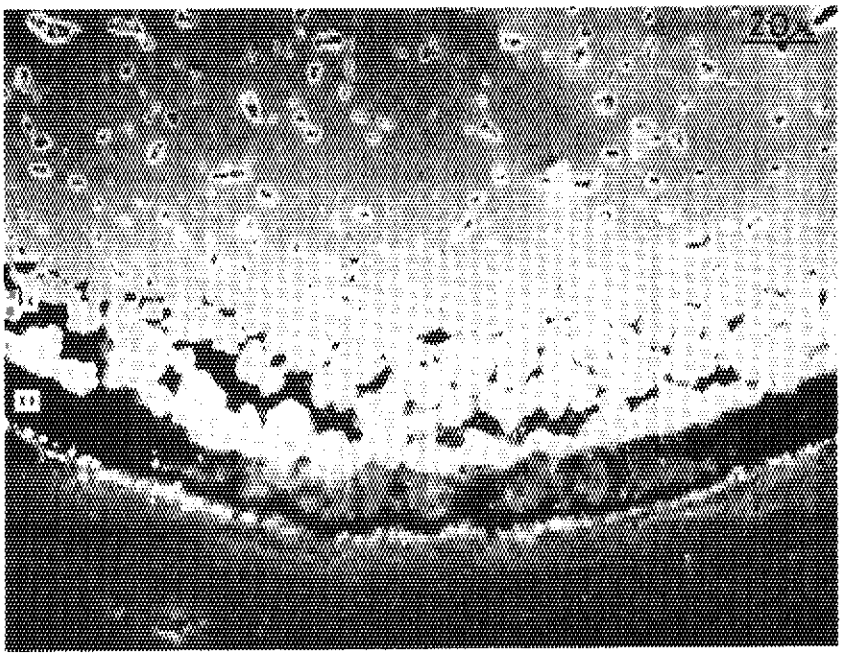

Fig. 13 Carbon precipitates along the grain boundaries of UO_2 kernel of 74UC1-3B particle.

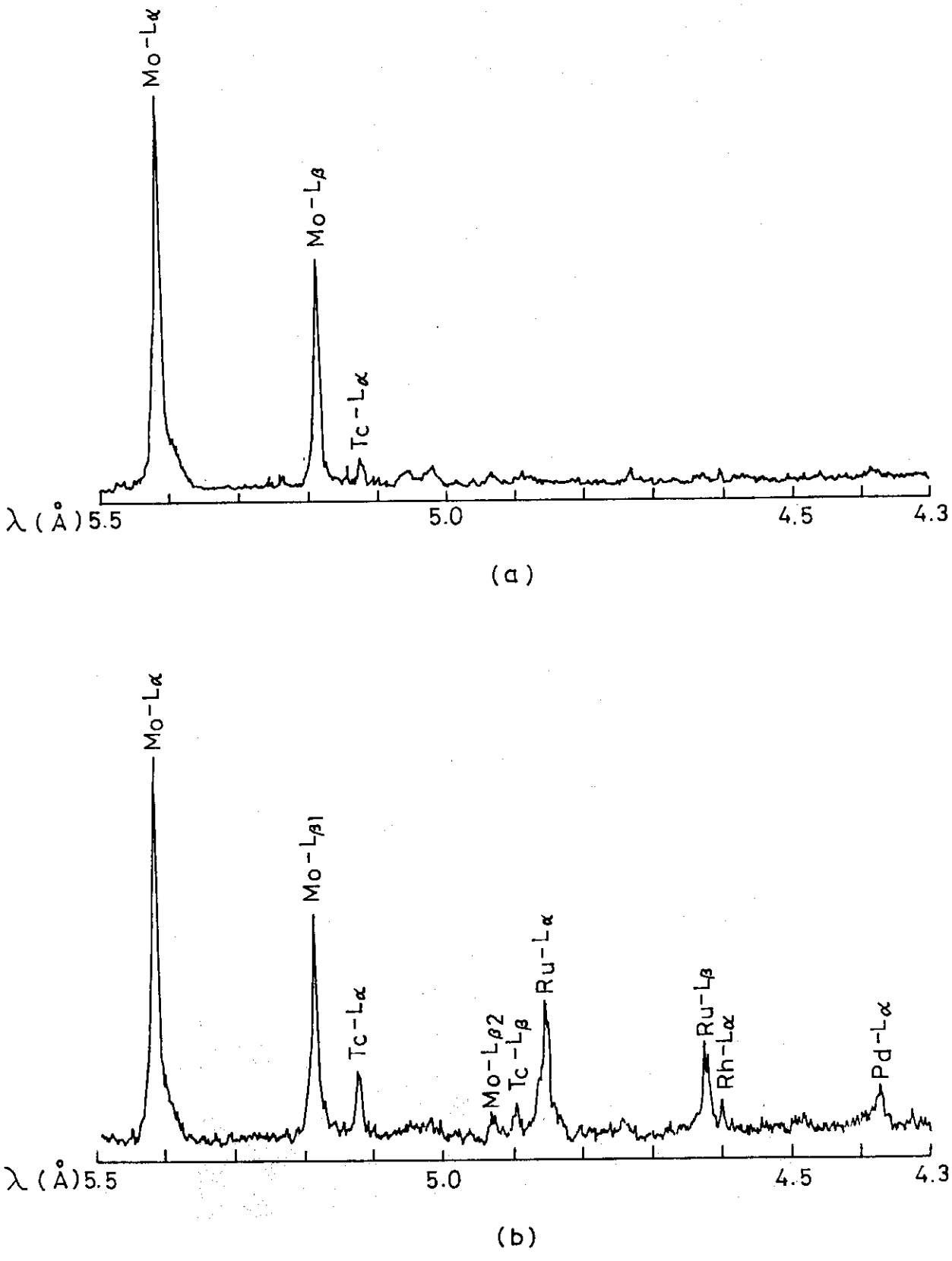

Fig. 14 X-ray spectra from the alloy inclusions of 74FCl-3A particle.

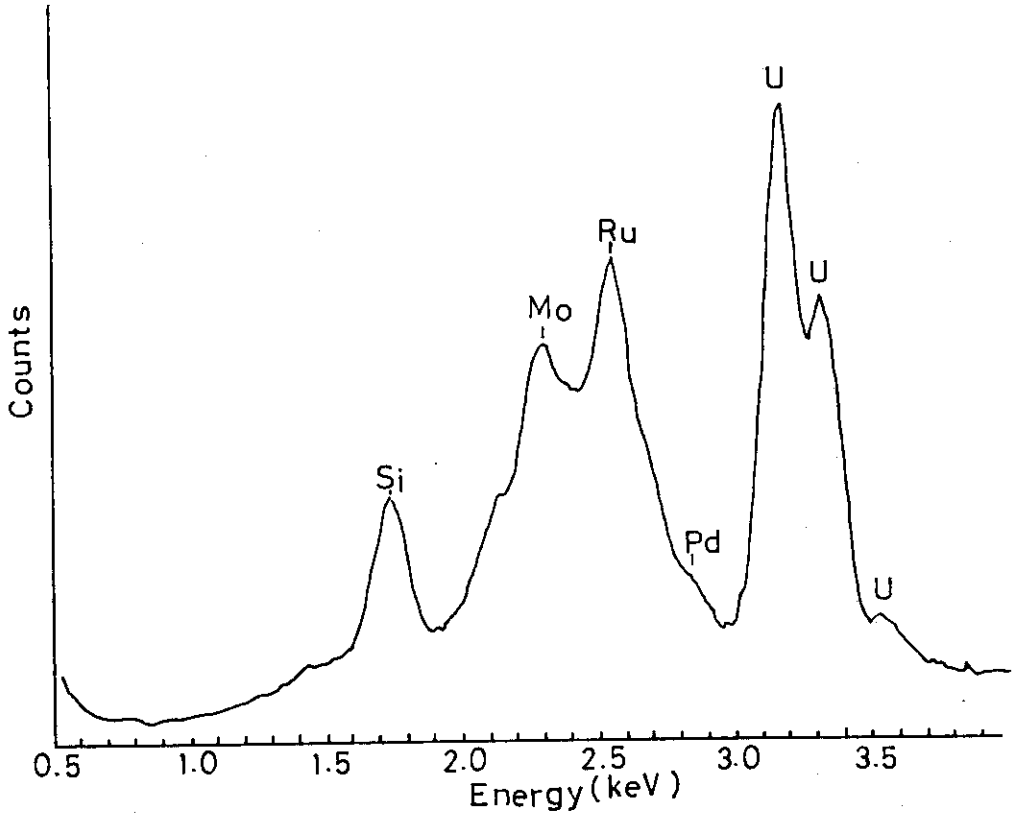

(a)

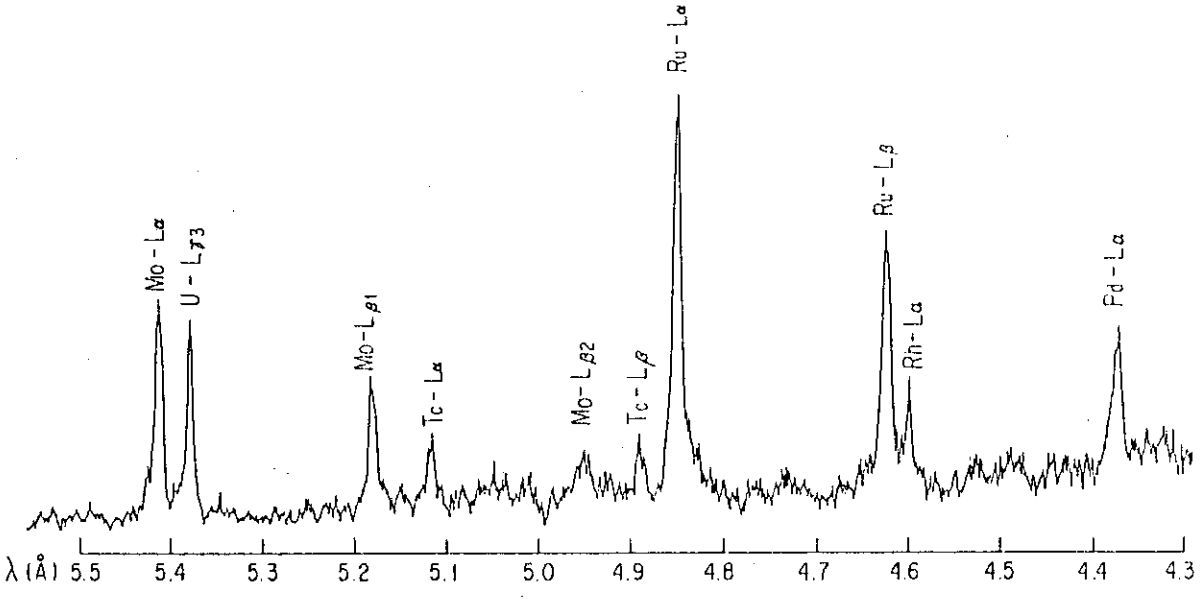

(b)

Fig. 15 X-ray spectra at the point of Si peak of the inclusion of Fig. 14b. a)EDX, b)WDX.

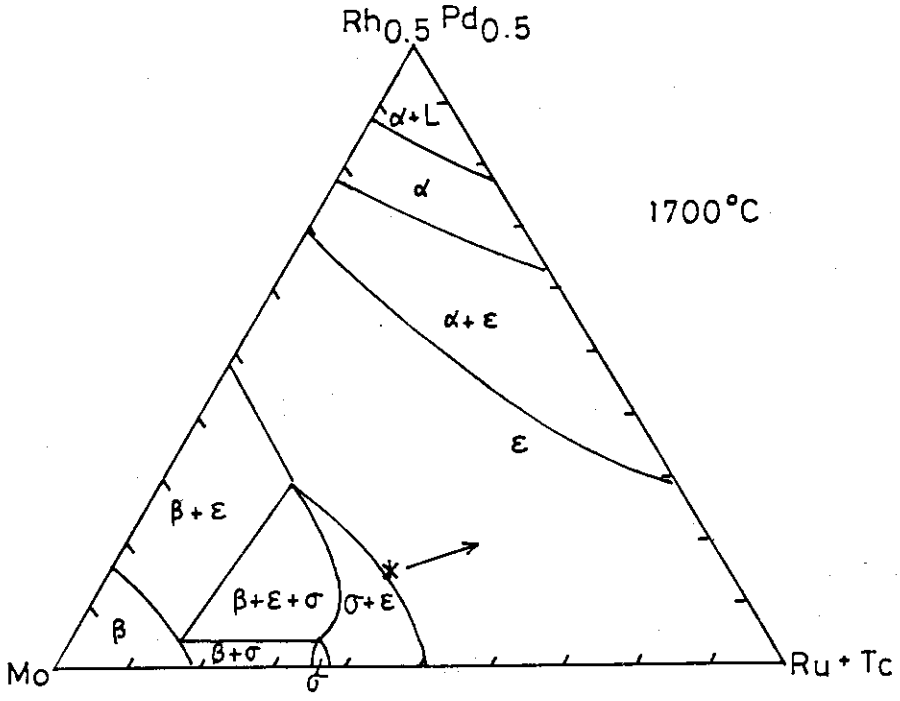

Fig. 16 Phase diagram of Mo-Ru(Tc)-$Rh_{0.5}Pd_{0.5}$ pseudo-ternary system[16]. Asterisk shows the approximate position expected for 74FCl-3A particle. Partial oxidation of Mo would shift the composition as shown by arrow.

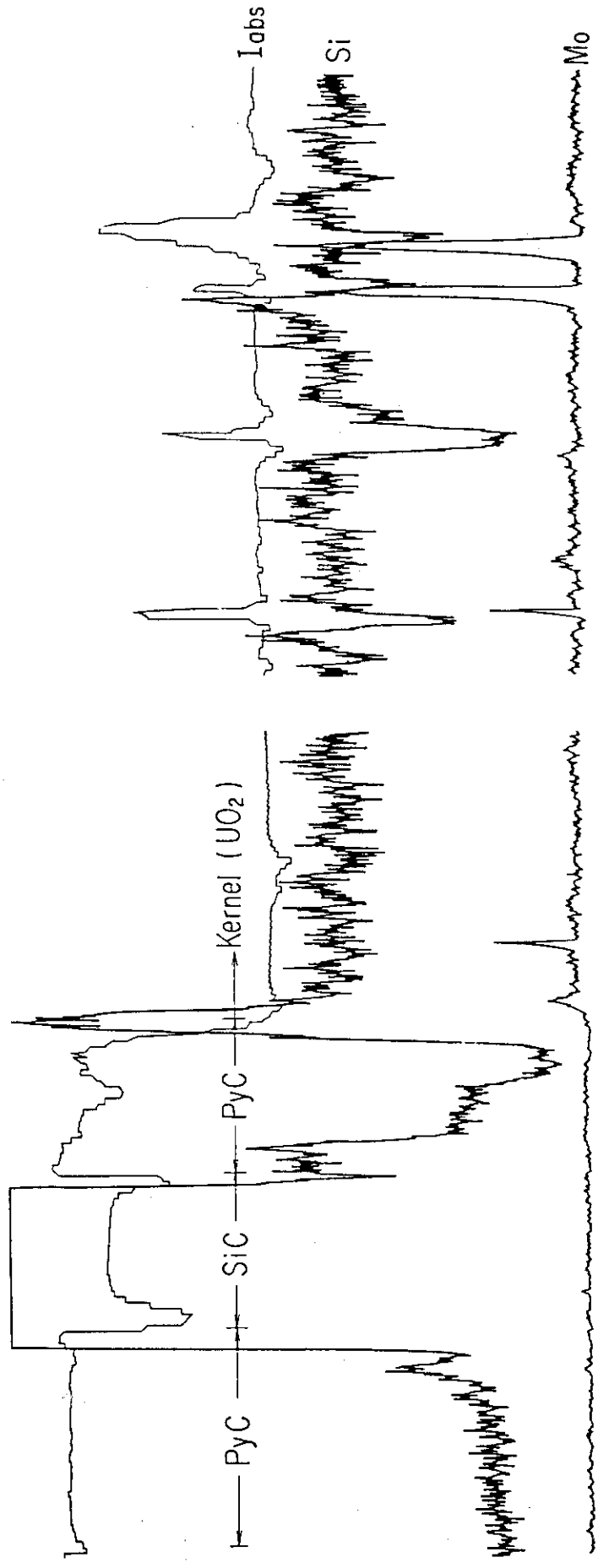

Fig. 17 Si distribution in 74FC1-3A particle.

	74FC1-3A	74FC1-5A
%FIMA	4.4	3.9
%fission in Pu	26	23
Bound oxygen (% of total O_2)		
(Sr,Ba)O	0.321	0.288
ZrO_2	1.227	1.101
$(Y,RE)_2O_3$ or $(Y,RE)O_2$	1.708 or 2.277	1.522 or 2.029
MoO_2	0.37 - 0.56	0.47 - 0.94
SiO_2	0.2 - 0.3	0.6 - 0.9
Total	3.83-4.12 or 4.40-4.69	3.98-4.75 or 4.49-5.26
Free oxygen (% of tatal O_2)	0.57-0.28 or none	none

Fig. 18 Account of oxygen balance in the particles 74FC1-3A and 5A.